Desalination and Water Treatment
www.deswater.com
18 (2010) 139–150
June
1944-3994 / 1944-3986 © 2010 Desalination Publications. All rights reserved.
doi: 10.5004/dwt.2010.1382

Towards optimization of spacer geometrical characteristics for spiral wound membrane modules

C.P. Koutsou, A.J. Karabelas*

Chemical Process Engineering Research Institute (CPERI) Centre for Research and Technology – Hellas (CERTH)
6th Km Charilaou-Thermi Road, PO Box 6036, Thermi-Thessaloniki, 57001, Greece
Tel.: +30 2310 498181; email: karabaj@cperi.certh.gr

Received 1 July 2009; Accepted 5 October 2009

ABSTRACT

Key parameters in the design of spiral wound elements are the geometrical characteristics of net-type spacers at the feed-flow channels, which greatly influence the transport phenomena therein and the overall operation of these modules. Recent results from a comprehensive theoretical and experimental study, on the flow characteristics and mass transfer in narrow channels with spacers, summarized in this paper, provide basic information that enables optimization of spacer characteristics. The new results include correlations of pressure drop and of average mass transfer rates to the wall as well as distributions of local shear stress and mass transfer, as a function of Reynolds and Schmidt number and of spacer geometry. An assessment of spacers, based on the above results, indicate trends, regarding geometric parameter values, leading to improved membrane element performance. Numerical results are also presented of an example, involving a single element in a RO seawater desalination plant, which demonstrate the applicability of the proposed new expressions for optimizing spacer and system performance. Finally, it is argued that an "optimum" spacer geometry depends on the kind of membrane operation (RO, NF, UF) employed to treat feed water of specific characteristics, which implies that most likely there exists no single spacer geometry with universally optimum performance.

Keywords: Spiral wound membrane elements; Spacers; Pressure drop; Shear stresses; Mass transfer coefficients; Optimization of performance

1. Introduction

Spiral wound membrane (SWM) modules are predominantly used in advanced processes for water desalination and treatment of various effluents. This kind of module is equipped with a net-type polymeric material (spacer), placed in-between neighboring membrane leaves, to create the necessary space for feed water flow. Spacers tend to promote the development of turbulence and to increase the wall shear stresses that lead to reduction of the undesirable phenomena of concentration polarization and of membrane fouling and scaling. However, they also contribute to increased pressure drop and energy expenditure, and possibly to the creation of limited- (or dead-) flow zones if not properly designed. Therefore, the spacer geometrical characteristics are the key design variables in the typical optimization problem emerging due to the aforementioned opposite trends, associated with the flow in the narrow feed channels. Indeed, the spacer geometrical parameters as well as the flow rate essentially determine the transport phenomena (momentum and mass transfer) within the complicated geometry of the narrow feed channels.

*Corresponding author.

This paper is part of a comprehensive study aimed at obtaining an improved understanding of transport phenomena in SWM elements, and at optimizing spacer design by identifying geometries associated with sufficiently high mass transport coefficients at relatively low pressure drop. The spacers considered in this study consist of two arrays of parallel unwoven thin cylindrical filaments (in contact with each other), which intersect at a certain angle, β, and are in contact with both channel walls which represent the membranes. This geometry closely resembles currently used commercial spacers within the feed-side SWM channels. The flow field and mass transfer in such complicated narrow passages is influenced by physical and geometrical parameters such as the Reynolds and Schmidt numbers, cylindrical filament diameter D, distance between the filaments L, their intersection angle β, and the angle of flow orientation α.

There is a significant amount of theoretical and experimental work in the literature, dealing with the study and optimization of spacer geometrical characteristics. Studies relevant to the present paper include that of Li et al. [1], who investigated flow characteristics and mass transfer in spacer-filled channels, by performing 3D simulations. Spatially periodic boundary conditions were imposed which allowed the study of the aforementioned phenomena in a spacer unit cell. The influence of spacer geometry on pressure drop and mass transfer was studied and some optimum geometries were suggested. These results, for which no information about the time and spatial discretization was provided, were compared with experimental data, and good agreement was reported [2,3]. Da Costa et al. [4–6] performed experiments with commercial and laboratory-made spacers to obtain data on pressure drop and flux [4–6], as well as mass transfer coefficients, using UF membranes [4,5]. Working with idealized geometries comprised of a set of parallel filaments, as well as with a variety of commercial spacers, Da Costa and Fane [6] showed that filaments attached to the membrane and transverse to the mean flow (the ladder-type spacer) are more effective in reducing concentration polarization and more economically attractive than filaments aligned with the flow. They also suggested that an optimum mesh length exists.

This paper is based on the results of a comprehensive study aiming to compliment and significantly extend the aforementioned as well as other works in the literature. Specifically, the study includes 2-D [7] and 3-D [8] *direct numerical simulations* of the fluid flow, as well as 3-D simulations of the mass transfer [9], in the above described narrow channels, by considering spacers in a rather broad geometrical parameter space. In conjunction with the numerical studies a significant amount of measurements were obtained of pressure drop [8] and of space-averaged mass transfer coefficients [9], in a specially made experimental set-up, for comparison with the theoretical predictions. The new data from numerical simulations and experiments on pressure drop, wall shear stresses and mass transfer coefficients, in the form of generalized correlations for various spacer geometries, provide the basis for optimizing spacer geometrical characteristics and the performance of SWM elements. Numerical and experimental techniques, used in this study, are outlined first and the main results are summarized later. Regarding optimization of spacer geometrical parameters, general considerations are discussed and trends are identified for optimum membrane module performance, on the basis of the new results. Finally, an example is provided demonstrating the applicability of the new results to spacer and performance optimization of a RO element.

2. Numerical simulations

The flow geometry considered is a close approximation of the narrow channels with spacers which are formed in spiral wound elements at the concentrate side. It consists of a flat narrow channel in which a net is placed, comprised of two layers of non-woven straight cylindrical filaments of diameter D. The filaments of each layer are parallel and equidistant, whereas the two layers have different orientation and intersect at a certain angle, β. The channel height (H) is twice the cylinder diameter ($H = 2D$). In Figure 1, a top view of the spacer is provided. The geometrical characteristics of a spacer include the ratio of the distance between parallel filaments to the filament diameter (L/D), the angle between the crossing filaments β, and the flow attack angle α.

It is considered that fluid flow development exhibits a periodicity in each cell, which is formed by four neighboring cylindrical filaments (indicated as ABCD in Figure 1); therefore, the flow is studied in a unit cell

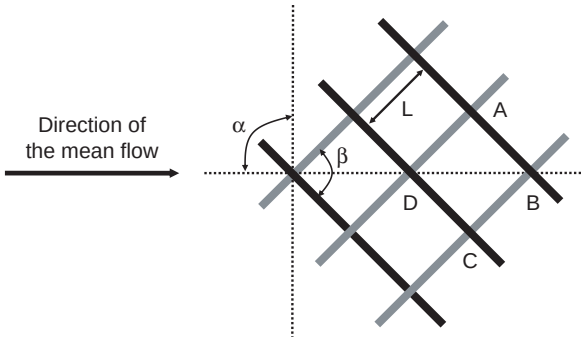

Fig. 1. The geometrical characteristics of net-type spacers; top view.

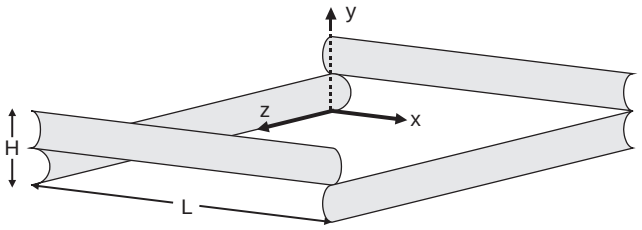

Fig. 2. The geometry of the 3D-simulations of the flow filed and mass transfer.

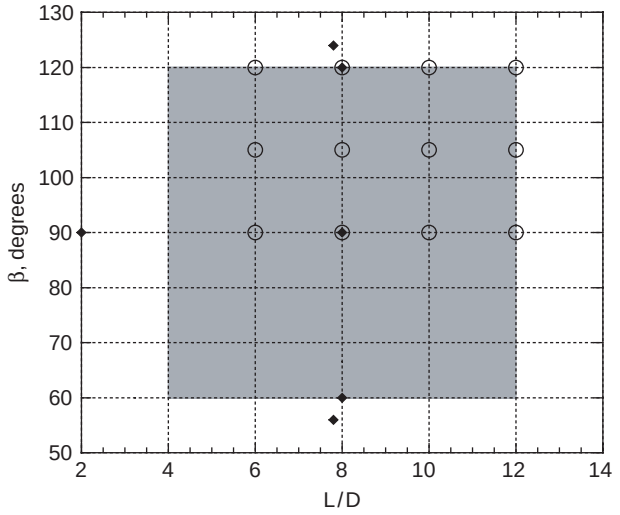

Fig. 3. The shaded area depicts the geometrical parameter space of commonly employed RO membrane feed spacers. Squares represent previous theoretical studies [1] in the literature for α = 90°. Circles represent the geometrical parameters considered in this work.

(a parallelepiped), that includes half of each of the four cylinders, in which periodic boundary conditions are applied (Figure 2).

In commercial spacers the ratio L/D usually varies between 7 and 9, while the angles α and β are in the range of 0° to 90° and 60° to 120°, respectively [4–6, 10–13]. It should be pointed out that if the mean flow is not symmetrically oriented with regard to the spacer configuration (i.e. if α is not 90°) an asymmetry between the two channel surfaces exists, regarding the flow and mass transfer characteristics. This asymmetry may lead to different concentration polarization and fouling behavior for the two membrane surfaces comprising the flow channel, which is not desirable. For this reason, in all the flow field simulations, presented in a previous paper [8], as well as in mass transfer simulations [9], the orientation of the spacer is taken to be symmetric with regard to the main flow direction, so that α = 90°. The geometrical parameter space of flow simulations is depicted in Figure 3. Existing results from previous theoretical studies in the literature for α = 90° are marked in the same figure. Apart from these numerical studies, there are also some experimental studies in the literature for α = 90° [2–6,10,12], some of which are referred to in the Introduction. As shown in Figure 3, the flow field simulations of the present study, including additional cases at L/D = 10 (with β = 90°, 105°, 120°) not reported in a previous paper [8], do not repeat the results of previous theoretical studies but significantly extend them. It should also be noted that in this work the angle β is taken equal to or larger than 90°. This is because when the filament orientation tends to become parallel to the mean flow direction, inferior mass transfer performance is obtained, namely lower mass transfer coefficients for the same Reynolds and Schmidt numbers, as suggested by several previous experimental [4,12] and theoretical studies [1]. In Table 1, all the simulations concerning the flow field and mass transfer are listed, with the corresponding geometrical characteristics of spacer configurations.

Flow and mass transport are governed by Navier-Stokes, continuity and mass transfer equations, assuming that the fluid is Newtonian and incompressible.

$$\frac{\partial \boldsymbol{u}}{\partial t} + \boldsymbol{u}.\nabla \boldsymbol{u} = -\nabla P + \frac{1}{Re}\nabla^2 \boldsymbol{u} \tag{1a}$$

$$\nabla.\boldsymbol{u} = 0 \tag{1b}$$

$$\frac{\partial C}{\partial t} + \boldsymbol{u}.\nabla C = \frac{1}{Pe}\nabla^2 C \tag{1c}$$

Table 1
Geometrical parameters of the flow and mass transfer simulations.

	Flow field simulations			Mass transfer simulations	
	β = 90°	β = 105°	β = 120°	β = 90°	β =120°
L/D = 6	Case study 1	Case study 5	Case study 9	Case study 13	Case study 15
L/D = 8	Case study 2	Case study 6	Case study 10	Case study 14	
L/D = 10	Case study 3	Case study 7	Case study 11		
L/D = 12	Case study 4	Case study 8	Case study 12		

It is emphasized that the results in this study are obtained through a *direct numerical simulation (DNS)* involving equations (1a) to (1c), without the introduction of any approximation for turbulence modeling. A commercial CFD code (FLUENT, v. 6.2.16) is used, which employs the finite-volume method. In each simulation the governing equations are integrated in time by imposing a constant mean-pressure gradient until the flow and the concentration reach a statistically steady state.

The channel walls are considered to be impermeable because the RO permeation velocities are much smaller than the feed flow velocities, justifying this assumption. However, it should be pointed out that this assumption may be satisfactory for the fluid flow simulations, but not necessarily for the mass transfer problem; thus in future simulations, permeation needs to be considered in order to assess its significance. Consequently, the boundary conditions are the no-slip and no-penetration conditions on the channel surfaces and similarly on the space filament surfaces. In addition, for the mass transfer simulations, channel walls are assumed to be of uniform wall concentration, C_w. As mentioned before, flow and mass transfer are assumed to be periodic in each unit cell indicated in Figure 1. More details regarding the periodic fluid flow and mass transfer simulations are provided elsewhere [8,9].

The physical parameters of the fluid flow and mass transport in spacer filled channels, are the Reynolds, Schmidt and Sherwood numbers defined here as follows.

$$\mathrm{Re} = \frac{U \cdot D}{v}, \qquad Sc = \frac{v}{\mathcal{D}}, \qquad Sh = \frac{k \cdot D}{\mathcal{D}}$$

where

U : mean superficial velocity in the channel [m/s]
D : spacer filament diameter [m]
v : water kinematic viscosity [m^2/s]
D : salt diffusivity [m^2/s]
k : mass transfer coefficient [m/s]

Under typical conditions in spiral wound membrane elements, the velocity in the channels created by two adjacent membrane leaves and separated by the spacer does not exceed 0.4 m/s and the allowable pressure drop, recommended by manufacturers, should not exceed 0.6 bar/m [14]. Therefore, the Reynolds number, defined on the basis of the superficial velocity and the spacer filament diameter, is less than 200. Typical Schmidt numbers for brackish and sea water are of the order 10^3. In this series of mass transfer simulations, the Schmidt number values varied from 1 to 100; limitations associated with available computer power did not allow calculations at higher Sc. More specifically, at such large Schmidt numbers, the concentration boundary layers at the channel walls are very thin, necessitating a very fine grid which leads to significantly increased computational load. The latter exceeds our computer hardware capabilities.

3. Experimental

A schematic diagram of the experimental set-up is shown in Figure 4; this set-up, with appropriate adaptations, was used for both mass transfer and pressure drop measurements. A test section in the form of a flat narrow channel with impermeable walls has been constructed,

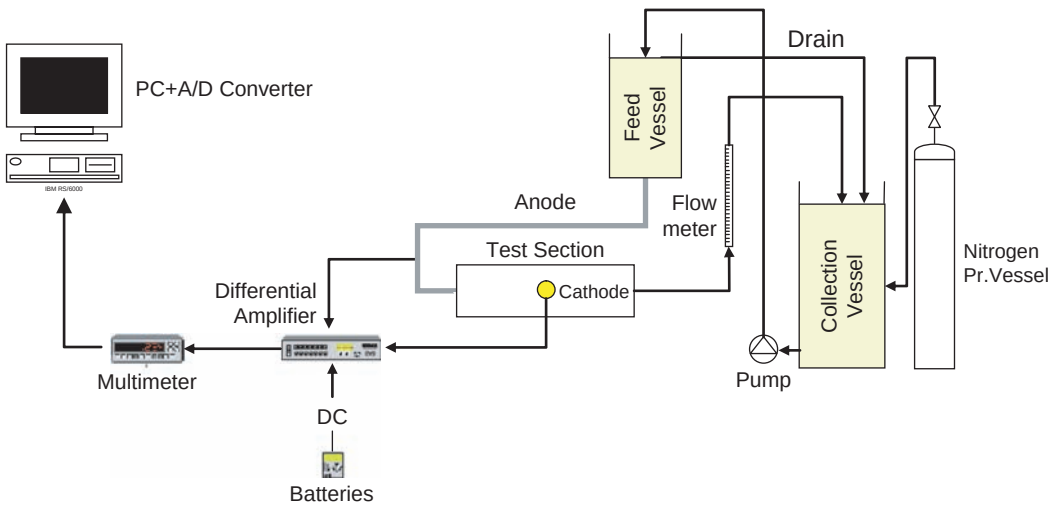

Fig. 4. A schematic diagram of the experimental set-up, for mass transfer measurements.

bearing features such as adjustable gap for precisely fitting the spacers and the specially fabricated electrodes for mass transfer measurements. The test channel is comprised of two thick Plexiglass plates on which special features for smooth flow entry and exit, as well as for flow development, have been machined. The free-flow length and width in the channel are 40 cm and 14.5 cm, respectively. In order to have a pulse-free flow, the feed vessel is elevated relative to the channel to provide the desired hydrostatic pressure. The fluid is collected in a second vessel after passing through the test section and is pumped back to the feed vessel.

For measuring mass transfer coefficients, a well-known electrochemical technique was used which was developed by Hanratty and collaborators [15]. This method also known as polarization technique is based on an electrochemical reaction which is controlled by the rate of mass transfer (through diffusion) to a sufficiently small electrode (cathode), embedded on a solid surface, over which convective flow exists. This non-invasive technique has been widely used for mass transfer and shear stress determination in single-phase flows in tubes [16] as well as for mass transfer studies in single and two-phase flows in complicated geometries such as packed beds [17,18]. The anode of the electrochemical system is a 2-inch stainless steel tube which connects the feed vessel with the test section, while the cathode is a circular disc, 40 mm in diameter made of bronze. It is flush-mounted with the upper channel wall and its surface is gold plated. The surface of the gold-plated cathode covers an adequate number of specially made spacer cells, which (depending on the spacer geometry) vary between 8 and 33. In the case of a common commercial spacer the number of spacer cells covered by the cathode is in excess of 140. More details about this technique, as implemented in this study, are provided elsewhere [9].

Polyethylene filaments of diameter 1 mm were glued together to create a variety of nine spacer patterns with characteristics similar to those of the flow field [8] and mass transfer simulation studies [9] carried out in this laboratory. Additional measurements were taken with a common commercial spacer, employed in Osmonics (AG4025T) elements, and characterized by angle β = 90° (square cell) and L/D ~ 10.

4. Results and discussion

4.1. Pressure drop

Pressure drop, which is related to the energy expenditure in membrane operations, has been computed and found to depend both on the ratio L/D and the angle β between spacer filaments. More specifically, pressure drop tends to decrease with increasing ratio L/D as the resistance to flow tends to be smaller for the less dense spacers (corresponding to greater channel void fraction ε). In addition, pressure drop increases with increasing angle β; this trend may be attributed to increased drag forces on the filaments as the angle β increases (towards β ~180°) and the angle of attack of the main flow tends to be normal to the filaments (as indicated in Fig. 1). For geometries which differ in both the ratio L/D and angle β, pressure drop is found to be larger for the geometry with the smaller ratio L/D, i.e. for the more dense spacers. In Figure 5 the dimensionless pressure drop, defined as $\left\langle \frac{\Delta P}{\Delta L} \right\rangle = \frac{\Delta P}{\Delta L} \cdot \frac{D}{U^2 \rho}$, is shown as a function of Reynolds number for the geometries of interest; in Table 2, the corresponding pressure drop correlations are presented. The theoretical predictions of pressure drop were

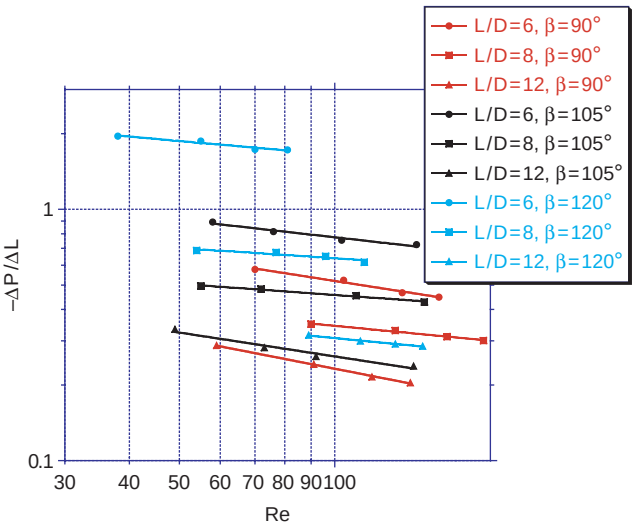

Fig. 5. Calculated dimensionless pressure drop as a function of Reynolds number for the geometries considered.

Table 2
Correlations between pressure drop and Reynolds number, from results of simulations.

	β = 90°	β = 105°	β =120°
L/D = 6	$-\Delta P/\Delta L = 2.3\ Re^{-0.31}$	$-\Delta P/\Delta L = 2.2\ Re^{-0.23}$	$-\Delta P/\Delta L = 3.8\ Re^{-0.18}$
L/D = 8	$-\Delta P/\Delta L = 0.8\ Re^{-0.19}$	$-\Delta P/\Delta L = 0.9\ Re^{-0.15}$	$-\Delta P/\Delta L = 1.2\ Re^{-0.14}$
L/D = 12	$-\Delta P/\Delta L = 1.5\ Re^{-0.40}$	$-\Delta P/\Delta L = 1.1\ Re^{-0.31}$	$-\Delta P/\Delta L = 0.7\ Re^{-0.19}$

compared with experimental measurements performed in this work, as well as with experimental and theoretical results from the literature, and good agreement was observed [8].

4.2. Local wall shear stresses and mass transfer coefficients

The results of the numerical simulations reveal the influence of spacer geometry on Sh number distributions. As shown in Figure 6 these distributions tend to be displaced towards smaller Sh values as the ratio L/D is increased, and towards higher values as the angle β is increased. Additionally, the local Sh distributions appear to be significantly broader at higher angle β.

In Figure 7, images are presented of the time-averaged spatial Sh distributions in comparison with the corresponding shear stresses. The results of this comparison indicate that mass transfer coefficient and wall shear stress distributions are similar and exhibit minimum and maximum values almost at the same locations of the unit cell surface, as shown in Figure 7. As seen

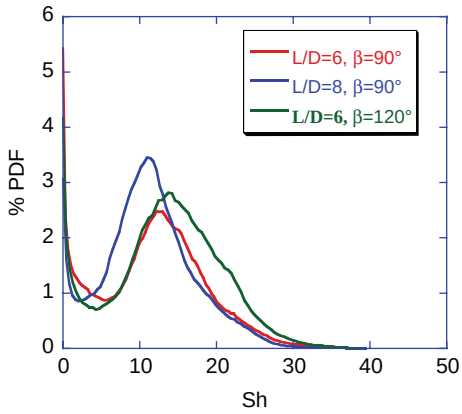

Fig. 6. Probability density functions of the time-averaged local Sherwood number at the channel walls, Re~80 and Sc = 1.

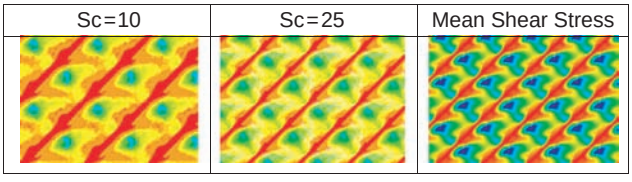

Fig. 7. Distribution of local values of time-averaged mass transfer coefficient and wall shear stress, for the channel top wall. Spacer geometrical characteristics: L/D = 6, β = 90°. Mean flow direction from left- to right-hand side. Note that red and blue colors correspond to minimum and maximum values respectively for the mass transfer coefficients, Re = 80.

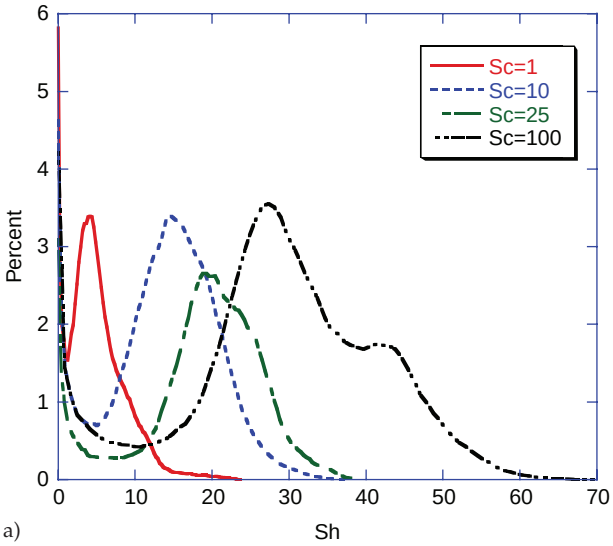

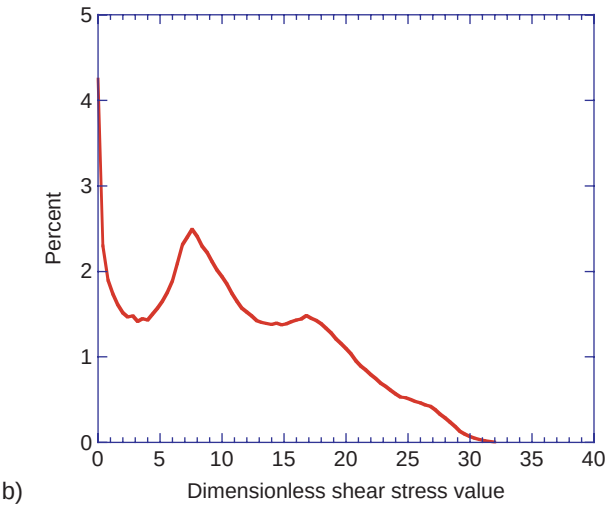

Fig. 8. Distribution of local time-averaged values of (a) Sherwood number for Sc = 1, 10, 25 and 100 and (b) Dimensionless shear stress, at the surface of the channel walls, for Re = 159. Parameter values: L/D = 6, β = 90°.

in Figure 8, with increasing Schmidt number the form of local mass transfer coefficient distribution tends to resemble closer the corresponding distribution of the local time-averaged shear stress values. This is attributed to the fact that, as the Schmidt number is increased, the concentration boundary layer tends to become thinner and as a consequence the mass transfer, at the channel walls, is affected more by the flow conditions near the channel surface than from the bulk.

4.3. Average mass transfer coefficients

In Figures 9 and 10, numerical and experimental results are presented concerning the effect of the Re and Sc numbers on Sh number, indicatively for one spacer

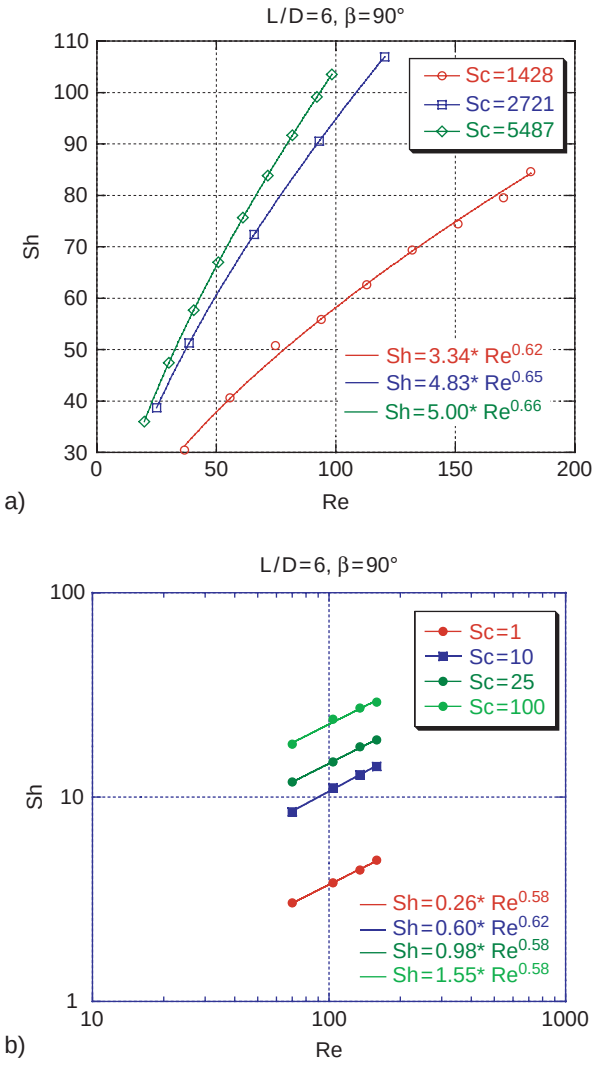

Fig. 9. The effect of the Re number on Sh number determined by (a) Experiments and (b) Numerical simulations.

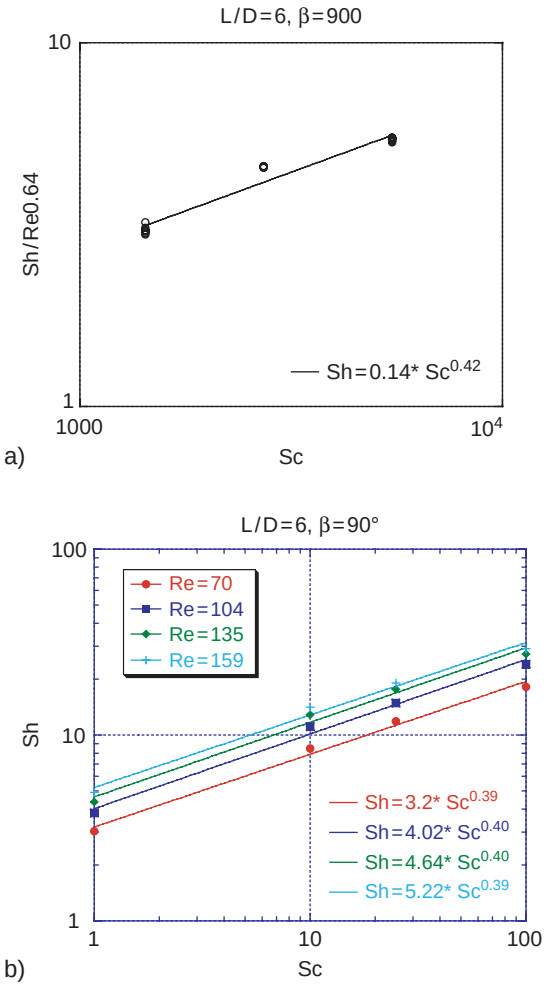

Fig. 10. The effect of the Re number on Sc number determined by (a) Experiments and (b) Numerical simulations.

geometry. It is observed that the exponent of Sh number dependence on Re number is quite similar for all the Sc numbers for which measurements were made. The same also holds true for the exponent of Sh dependence on Sc number, which is nearly constant for the Re range of the measurements. This result, which is confirmed for all the spacer geometries considered in the present study [9], allows the correlation of Sh with Re and Sc numbers. These correlations are presented in Table 3. It must be pointed out that the present study is the first one systematically examining the effect of both the Re and Sc numbers on Sh number, whereas all previous works are restricted to studying the effect of the Re number for a single Sc number. Upon inspection of Table 3, it is concluded that for spacer geometries with β = 90°, the exponent for the Reynolds number dependence is

Table 3
Correlations of measured average Sherwood number dependence on Re and Sc number, for all prototype spacer geometries considered in this work.

	β = 90°	β = 105°	β =120°
L/D = 6	$Sh = 0.14Re^{0.64}Sc^{0.42}$	$Sh = 0.08Re^{0.715}Sc^{0.48}$	$Sh = 0.073Re^{0.87}Sc^{0.45}$
L/D = 8	$Sh = 0.16Re^{0.605}Sc^{0.42}$	$Sh = 0.17Re^{0.625}Sc^{0.42}$	$Sh = 0.12Re^{0.71}Sc^{0.43}$
L/D = 12	$Sh = 0.26Re^{0.57}Sc^{0.37}$	$Sh = 0.17Re^{0.64}Sc^{0.40}$	$Sh = 0.19Re^{0.645}Sc^{0.38}$

around 0.6. This exponent tends to increase with angle β. It is also noteworthy that the exponent of the Sc number dependence is essentially constant, around 0.40. More information, including comparisons showing good agreement between numerical simulation results and experimental data from this study, as well as comparisons with other literature correlations are presented elsewhere [9].

5. Effect of spacer geometry on spiral wound module performance

5.1. General considerations

The adopted methodology in this study and in particular the results concerning pressure drop, wall shear stresses, and mass transfer coefficients, provide the necessary information for developing quantitative criteria towards optimization of spacer geometrical characteristics. For determining an *optimum* (or near-optimum) *spacer geometry*, one should take into consideration the effects of three parameters—*feed flow pressure drop* which directly affects energy expenditure, *mass transfer rates* of dissolved species to the wall which strongly influence concentration polarization, and *shear stresses* at the membrane surface, which (in addition to transport phenomena) affect membrane fouling. Spacer optimization should be based on quantitative criteria concerning the above parameters.

As far as establishing *pressure drop criteria*, this is feasible because estimation of energy expenditure due to pumping of feed is rather straight-forward. It must be noted that for relatively low-pressure processes treating low-salinity waters (LPRO, NF), where spiral wound elements usually operate in the pressure range 5 to 12 bar, differences in concentrate pressure drop because of different spacers, may have a significant impact on the energy efficiency of the entire process. Consequently, in this case, spacer ΔP characteristics should be estimated as accurately as possible for an optimization exercise. However, in RO desalination of seawater, where the operating pressure is usually in the range 60 to 70 bar, the same differences in pressure drop are expected to have a lesser impact on spiral-wound module operation. It appears, therefore, that the advantage of relatively smaller pressure drop, associated with certain spacer geometry, does not have the same impact on all membrane operations and feed water qualities.

On the basis of similar arguments, the impact of the spacer geometry on *mass transfer coefficients* should be taken into account, in a quantitative manner, for low and high salinity fluids. Based on reliable predictions of mass transfer coefficients, the concentration polarization and the osmotic pressure at the membrane surface can be calculated. One additional parameter is the concentration polarization of salts which tend to precipitate (e.g. Ca, Ba, Mg, etc) leading to deposits on the membrane surface. A relatively small concentration increase of these salts at the membrane surface could have a proportionately small impact on osmotic pressure, but may have a significant impact regarding the above species super-saturation and deposition, negatively affecting process operation as well as the cost of chemicals used for preventing scale formation. Quantification of this impact is necessary, and it is feasible with the improved expressions obtained in this work. Furthermore, it is obvious that variations of mass transfer coefficient due to spacer geometry would not have the same impact on all kinds of membrane processes, largely depending on the feed water characteristics. For instance, the osmotic pressure developing in membrane-filtered brackish waters is usually much smaller than that prevailing at the concentrate side of RO membranes treating seawater. Additionally, mass transfer considerations are of rather limited significance in UF operations. Consequently, the impact of improved spacer performance regarding mass transfer would be greater on RO than on NF and UF operations.

The phenomena of fouling are quite complicated and the impact of the spacer geometry thereon cannot be easily quantified, although one expects that the presence of higher shear stresses would be beneficial and would tend to extend the time intervals between successive membrane cleaning and as a consequence reduce the significant related costs, due to chemicals, downtime and water losses. Thus, one could employ at present qualitative criteria on this aspect, based on the new results.

To summarize the above considerations, the parameters of pressure drop and mass transfer coefficients could be rather easily utilized for the assessment of various spacer geometries, in a quantitative manner. Thus, taking advantage of the results obtained in this study, one can calculate the effects of varying the above parameters on the design and operation of membrane desalination plants, either by using various existing commercial software for membrane processes, or by developing novel accurate methods that appear to be necessary. Criteria, essentially qualitative, relating wall shear stresses to spacer geometries, obtained in this work, can supplement the above computational results. Finally, it should be stressed (as outlined above) that the "optimum" spacer geometry depends on the kind of membrane process considered, in relation to the specific characteristics of the feed water, which implies that very likely there exists no single spacer geometry with universally optimum characteristics.

5.2. The influence of spacer geometry on spiral wound element performance: An assessment of trends

Notwithstanding the above considerations on the "universally optimum" spacer geometry, the substantial amount of new results on pressure drop, local shear stress and local mass transfer computations, as well as the average mass transfer measurements, justify an assessment (albeit preliminary) of spacer geometric parameter values that may offer specific advantages regarding membrane element performance. For RO membrane operations, as outlined above, criteria that can be used for this assessment include pressure drop, space average wall shear stress and mass transfer coefficients as well as their distributions. In currently used commercial RO modules the spacer is usually characterized by parameters L/D~7–9 and $\beta = 90°$. The geometry of the present simulations closest to the above typical commercial spacer is $L/D = 8$, $\beta = 90°$. By inspection of Figure 5 one observes that pressure drop smaller than that of the typical commercial spacer appears to be associated with the greatest ratio L/D examined, i.e. $L/D = 12$, for all three angles β (90°, 105°, 120°).

These three cases can also be assessed on the basis of the measured space-averaged Sherwood number at the wall (Figure 11). The case $L/D = 12$, $\beta = 90°$, displays the smallest values of overall average Sh number (which is generally undesirable) but it is associated with the smallest pressure drop, while the cases $L/D = 12$, $\beta = 105°$ and $L/D = 12$, $\beta = 120°$, compared to the case $L/D = 8$, $\beta = 90°$, exhibit higher Sh numbers. The latter result is also verified by the computed space-averaged shear stress values at the wall, where the geometries $L/D = 12$, $\beta = 105°$ and $L/D = 12$, $\beta = 120°$ exhibit nearly the same and higher shear stress values compared to the geometry $L/D = 8$, $\beta = 90°$, respectively (Figure 12).

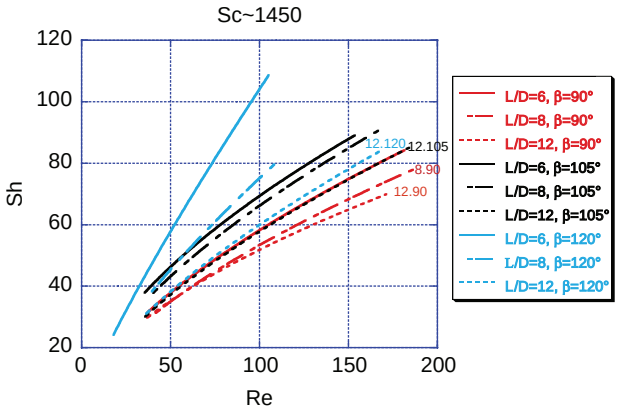

Fig. 11. Measurements of Sh number as a function of Reynolds number for the spacer geometries considered in this work, Sc~1450.

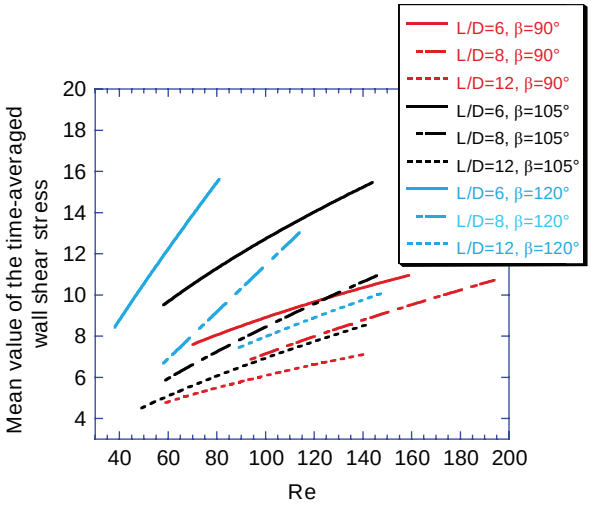

Fig. 12. Spatially mean values of the time-averaged wall shear stresses as a function of Reynolds number for all the geometries considered.

The above comparisons suggest that, overall, spacers with parameter values $L/D = 12$, $\beta = 90°$, may exhibit somewhat inferior performance compared to the other two cases with $L/D = 12$, i.e. $\beta = 105°$ and 120°.

Further comparative assessment of the last two cases ($L/D = 12$, $\beta = 105°$ or 120°) can be made on the basis of *distribution* of wall shear stress or Sh values. In Figure 13, the distribution of wall shear stress for the geometry $L/D = 8$, $\beta = 90°$ is shown in comparison to the corresponding distributions of the geometries $L/D = 12$, $\beta = 105°$ and $L/D = 12$, $\beta = 120°$. It is expected that a broader distribution of wall stresses with a greater percentage of relatively high values would be beneficial in reducing polarization effects and fouling. It should be noted first that the shear stress distributions are skewed to the right, with a significant percentage of near-zero values due to the contact lines and the nearly stagnant flow regions along these lines. Upon inspection of Figure 13, it appears that the geometry $L/D = 12$, $\beta = 120°$ is associated with a broader stress distribution which is advantageous (as outlined above), compared to the geometry $L/D = 12$, $\beta = 105°$ and to the geometry $L/D = 8$, $\beta = 90°$.

In conclusion, this assessment, based on the rather extensive flow simulations performed in this study as well as on the mass transfer data collected, suggests that, for applications such as RO where pressure drop, shear stresses and mass transfer rates play a significant role, spacer parameter values that appear to be associated with improved element performance may be near $L/D = 12$ and angle β closer to 120° than to 90°. It is evident that the above preliminary assessment provides trends that are subject to verification, through further

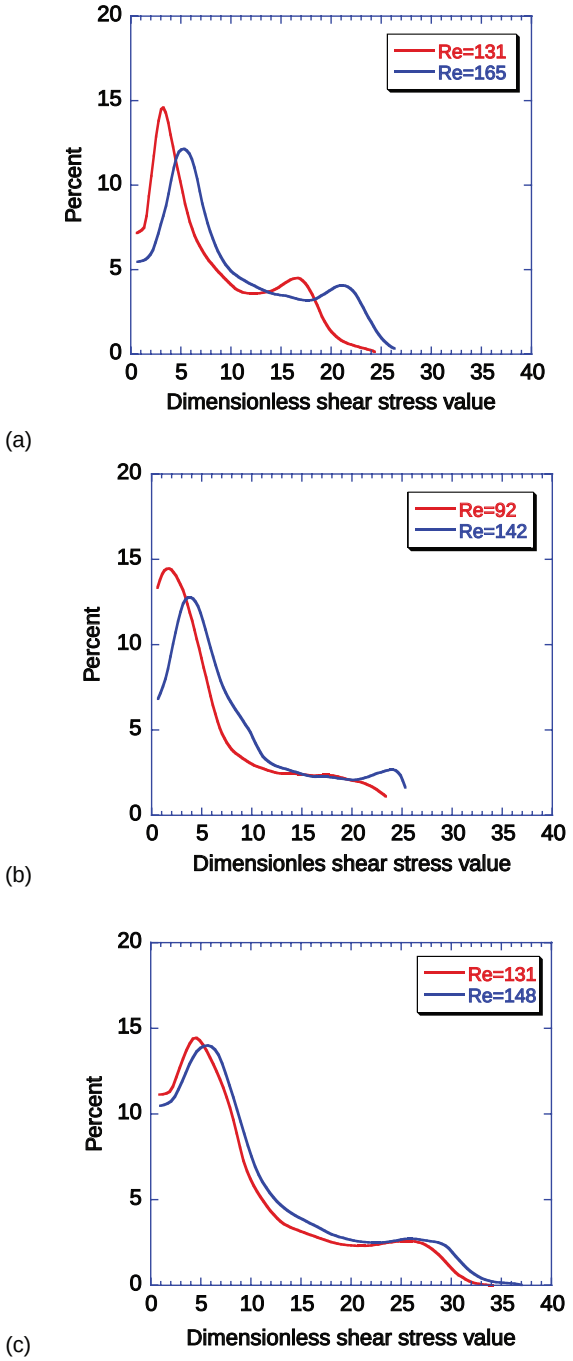

Fig. 13. Distribution of dimensionless shear stress values at the surface of the channel walls. Parameter values (a) L/D = 8, β = 90°, (b) L/D = 12, β = 105° and (c) L/D = 12, β = 120°.

experimental testing and numerical simulations. Additionally, the comments made above, regarding the different conditions and requirements of NF-LPRO and of high pressure RO processes, should be taken into account when the issue of spacer geometrical optimization is addressed.

5.3. An example of selecting optimum spacer geometry for RO elements, for sea water desalination

As discussed in the preceding section, the optimum spacer geometry apparently depends on the kind of membrane process considered, in relation to the specific characteristics of the feed water. Consequently, the issue of the optimum spacer geometry should be examined separately for each major category of membrane applications. An example is provided here for RO sea-water desalination, with a membrane that is not fouled, to demonstrate the usefulness of the new information developed in this study. To take into account quantitatively the effect of spacer geometry on pressure drop and concentration polarization, the following function is considered in the search of an optimum.

$$\frac{\Delta P_{eff}}{\Delta P_{nominal}} = \frac{\Delta P_{applied} - \Delta P_f - CP \cdot \Delta\pi}{\Delta P_{applied} - \Delta\pi} \quad (4)$$

where

$\Delta P_{applied}$: the applied trans-membrane pressure
ΔP_{eff} : the effective operating pressure difference
ΔP_f : the pressure drop at the feed water channel
CP : the concentration polarization factor
$\Delta\pi$: the osmotic pressure difference

Here, $\Delta P_{nominal}$, is the difference between the applied pressure and the osmotic pressure computed on the basis of bulk salt concentration, whereas the effective operating pressure difference is further reduced due to pressure drop in the feed channel and the concentration polarization. The latter effect may be quantified, as is common (e.g. [19]), by determining a concentration polarization factor $CP = \exp(J/k)$, where J is the trans-membrane flux and k the mass transfer coefficient, $k = \frac{Sh \cdot \mathcal{D}}{D}$, computed from the correlations of Table 3 that depend on the particular spacer geometry. To obtain specific numerical results, the pressure conditions prevailing at the end of the first element in an array (i.e. 1.0 m from feed entry) are estimated, for various spacer geometries. Typical process parameter values are employed for sea-water of salinity 35.000 ppm NaCl. The case of a typical-filament mean diameter 34mils is considered [20]. The various parameter values used in the calculations, typical for sea-water desalination, as well as other data are listed in Table 4.

In Figure 14, the ratio of effective over the nominal trans-membrane pressure is plotted as a function of feed-channel Reynolds number, for the various spacer geometries examined in this work. Figure 14 shows that for most spacer geometries there is a rather narrow range of near optimum operation (from the stand-point of effective pressure) characterized by Re numbers roughly

Table 4
Parameter values employed in the example of determining "optimum" spacer geometrical characteristics for RO elements, in sea-water desalination service.

$\Delta P_{applied}$	$\Delta\pi$	ΔP_f	J	Sh	$\mathcal{D}$	D	Sc
70 bar	26.7 bar	Table 2	20 L/m^{2}h	Table 3	1.2710^{-9} m^2/s (Salinity 35.000 ppm)	0.43mm (34 mils filament)	700

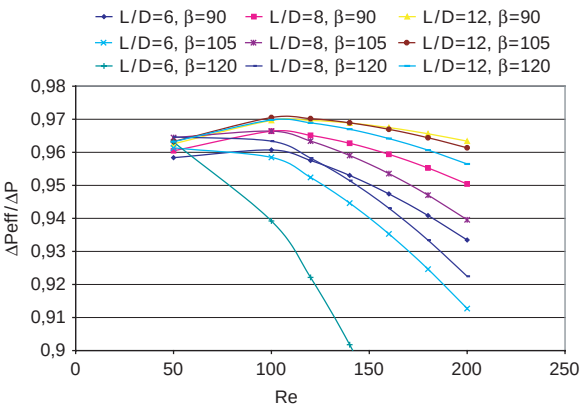

Fig. 14. The ratio of the effective over the nominal trans-membrane pressure as a function of the feed channel Re number.

100 to 120. At Re below 100, the mass transfer rates are relatively small and concentration polarization tends to enhance the effective osmotic pressure at the membrane surface, thus reducing the effective trans-membrane pressure; at Re above 120, pressure drop in the channel due to higher cross flow tends to become excessive and to eliminate any benefits resulting from the concomitant reduction of concentration polarization. It is further noted that, for the case considered, spacer geometries with L/D = 12 exhibit an optimum performance in comparison with the other geometries, i.e. the greatest values of effective over nominal trans-membrane pressure, which is in accord with the general trends suggested by the assessment of new results outlined in a preceding section. It should be finally pointed out that the cross-flow velocity corresponding to the Re range 100 to 120 (where the performance appears to be near optimum) is 0.23 to 0.28 m/s, that is within the commonly used operating velocities in commercial plants, and recommended by membrane element manufacturers.

6. Conclusions and discussions

Results are summarized of a numerical and experimental study, systematically examining the effect of Reynolds number (Re) on pressure drop and of Reynolds (Re) and Schmidt (Sc) numbers on Sherwood (Sh) number, for narrow channels with spacers, closely mimicking conditions in feed-side channels of spiral-wound modules. The numerical study comprised extensive 3D simulations of the fluid flow [7,8] and mass transfer [9], in spacer filled channels, for a relatively broad range of spacer geometrical parameters. The validity of the numerical results was confirmed by comparison with experimental data on pressure drop and average mass transfer rates. The results of this study confirm that pressure drop and mass transfer coefficients are strongly dependant on spacer geometry; in particular, these quantities tend to decrease with increasing ratio of L/D and to increase with the angle β. Additionally, for each geometry considered, correlations are obtained of $\Delta P/\Delta L$, and of average Sh number in terms of Re and Sc numbers; the exponent of Sherwood number dependence on Schmidt number is near 0.4.

An assessment of spacers (based on the results on wall shear stress and Sh distributions, as well as on pressure drop) indicates trends, regarding their geometrical parameter values, leading to improved membrane element performance in RO operations. More specifically, it appears that the less dense spacers studied (i.e. L/D = 12), with filament crossing angles β greater than 90°, may hold advantages over other commonly used spacer geometries. Results on shear stress distributions tend to support these trends regarding "near optimum" spacer parameters. It is argued, however, that an "optimum" spacer geometry apparently depends on the kind of membrane element employed (i.e. for RO, NF, or UF operation) to treat a feed-water with the specific characteristics regarding salinity and fouling propensity; this implies that very likely there exists no single spacer geometry with universally optimum performance. To test the validity of the above conclusions, results of a numerical example are reported to identify spacer geometries associated with optimum performance, for the case of a typical RO membrane element in sea water desalination. By taking into account the reduction of effective trans-membrane pressure caused by feed-flow pressure drop and by concentration polarization effects, as a function of Re, a narrow range of optimum spacer parameters and cross-flow velocities could be determined. The identified near optimum spacer parameters,

in this example, are in accord with the preceding qualitative assessment; moreover, the narrow range of optimum Re and cross-flow velocities identified are in agreement with membrane module manufacturers recommendations for operating RO systems. It should be pointed out, however, that in systematic spacer optimization calculations, one must take into account the axial variability of flow rate and salt concentration, along a pressure vessel, using appropriate software and the new correlations developed in this study.

To conclude, the new information obtained in this study (i.e. results of simulations and experimental data) provide a solid basis for further exploration of issues, related to optimization of spacers and of membrane module operating conditions. In particular, the new results clearly demonstrate the usefulness of advanced computational tools to predict flow characteristics and mass transfer in the complicated narrow channels examined here and, thus, to determine the performance of spacers in relation to their geometrical parameters. Therefore, in designing membrane modules for a specific operation (RO, NF or UF), systematic screening and selection of a narrow range of optimum spacer parameters appears to be possible with numerical techniques in lieu of expensive pilot plant experiments.

Acknowledgement

Grateful acknowledgement is made of financial support by the *Middle East Desalination Research Center*, under contract number 04-AS-002.

References

[1] F. Li, W. Meindersma, A.B. de Haan and T. Reith, Optimization of commercial net spacers in spiral wound membrane modules, J. Membr. Sci., 208 (2002) 289–302.
[2] F. Li, W. Meindersma, A.B. de Haan and T. Reith, Optimization of non-woven spacers by CFD and validation with experiments, Desalination, 146 (2002) 209–212.
[3] F. Li, W. Meindersma, A.B. de Haan and T. Reith, Experimental validation of CFD mass transfer simulations in flat channels with non-woven spacers, J. Membr. Sci., 232 (2004) 19–30.
[4] A.R. Da Costa, A.G. Fane, C.J.D. Fell and A.C.M. Franken, Optimal channel spacer design for ultrafiltration, J. Membr. Sci., 62 (1991) 275–291.
[5] A.R. Da Costa, A.G. Fane and D.E. Wiley, Spacer characterization and pressure drop modelling in spacer-filled channels for ultrafiltration, J. Membr. Sci., 87 (1994) 79–98.
[6] A.R. Da Costa and A.G. Fane, Net-Type spacers: Effect of configuration on fluid flow path and ultrafiltration flux, Ind. Eng. Chem. Res., 33 (1994)1845–1851.
[7] C.P. Koutsou, S.G. Yiantsios and A.J. Karabelas, Numerical simulation of the flow in plane channel containing a periodic array of cylindrical turbulence promoters, J. Membr. Sci., 231 (2004) 81–90.
[8] C.P. Koutsou, S.G. Yiantsios and A.J. Karabelas, Direct Numerical simulation of flow in spacer-filled channels: effect of spacer geometrical characteristics, J. Membr. Sci., 291 (2007) 53–69.
[9] C.P. Koutsou, S.G.Yiantsios andA.J. Karabelas, A numerical and experimental study of mass transfer in spacer-filled channels: Effects of spacer geometrical characteristics and Schmidt number, J. Membr. Sci., 326 (2009) 234.
[10] G. Shock and A. Miquel, Mass transfer and pressure loss in spiral wound modules, Desalination, 64 (1987) 339–352.
[11] O. Kuroda, S. Takahashi and M. Nomura, Characteristics of flow and mass transfer rate in an electrodialyzer compartment including spacer, Desalination, 46 (1983) 225–232.
[12] C.C. Zimmerer and V. Kottke, Effects of spacer geometry on pressure drop, mass transfer, mixing behavior, and residence time distribution, Desalination, 104 (1996) 129–134.
[13] S.K. Karode and A. Kumar, Flow visualization through spacer filled channels by computational fluid mechanics I. Pressure drop and shear stress calculations for flat sheet geometry, J. Membr. Sci., 193 (2001) 69–84.
[14] Hydranautics, RODESIGN, Hydranautics RO System Design Software, VERSION 6.4 (c). Pretreatment and design limits section of help module (1998).
[15] L.P. Reiss and T.J. Hanratty, Measurement of instantaneous rates of mass transfer to a small sink on a wall, A.I.Ch.E. J. 8 (1962) 245–247.
[16] J.E. Mitchell and T.J. Hanratty, A study of turbulence at a wall using an electrochemical wall shear-stress meter. J. Fluid Mech., 26 (1966) 199–221.
[17] N.A. Tsohatzidis and A.J. Karabelas, Study of pulsing flow in a trickle bed using the electrodiffusion technique, J. Appl. Electrochem., 24, (1994) 670–675.
[18] A.J. Karabelas, T.H. Wegner and T.J. Hanratty, Flow pattern in a close-packed cubic array of spheres near the critical Reynolds number, Chem. Eng. Sci., 73 (1973) 673–682.
[19] M. Mulder, Basic principles of membrane technology, 2nd ed., Kluwer Academic Publishers, Dordrecht, 1996.
[20] C. Bartels, M. Hirose, H. Fujioka, Performance advancement in the spiral wound RO/NF element design, Desalination, 221(2008) 207–214.